

# Simplified analytical Moment-Curvature relationship for hollow circular RC cross-sections

Roberto Gentile\* and Domenico Raffaele<sup>a</sup>

Department of Civil, Environmental, Land, Building Engineering and Chemistry, Polytechnic University of Bari, Bari, Italy

(Received April 15, 2018, Revised July 12, 2018, Accepted July 15, 2018)

**Abstract.** The seismic vulnerability analysis of multi-span bridges can be based on the response of the piers, provided that deck, bearings and foundations remain elastic. The lateral response of an RC bridge pier can be affected by different mechanisms (i.e., flexure, shear, lap-splice or buckling of the longitudinal reinforcement bars, second order effects). In the literature, simplified formulations are available for mechanisms different from the flexure. On the other hand, the flexural response is usually calculated with a numerically-based Moment-Curvature diagram of the base section and equivalent plastic hinge length. The goal of this paper is to propose a simplified analytical solution to obtain the Moment-Curvature relationship for hollow circular RC sections. This based on calibrated polynomials, fitted against a database comprising 720 numerical Moment-Curvature analyses. The section capacity curve is defined through the position of 6 characteristic points and they are based on four input parameters: void ratio of the hollow section, axial force ratio, longitudinal reinforcement ratio, transversal reinforcement ratio. A case study RC bridge pier is assessed with the proposed solution and the results are compared to a refined numerical FEM analysis, showing good match.

**Keywords:** Moment-Curvature; hollow circular cross-sections; reinforced concrete; RC members optimisation; RC bridge piers; seismic vulnerability

## 1. Introduction

Seismic vulnerability of existing bridge structures is a particularly relevant theme in earthquake-prone countries, given the need to have a vulnerability inventory for large infrastructures. Recent earthquakes, e.g., the 2016 Kaikoura earthquake in New Zealand (Palermo *et al.* 2017), demonstrated the crucial role of the road bridges in the aftermath of the earthquake, whose performance is desirable for the mitigation actions to take place. Therefore, regional-scale inventories of the seismic performance of bridges should be pursued.

Clearly, refined non-linear analyses is both time- and cost-ineffective for large portfolios (Pinho *et al.* 2009). Instead, multi-level approaches are preferred, starting with large-scale simplified analyses, creating a prioritisation scheme and refining the analysis only for the top-priority elements. Typically, large-scale analyses are based on semi-empirical calibrated indexes (Kircher *et al.* 2006). Other approaches are based on the definition of mechanically-based simplified capacity curves for classes of structures based on ideal case study bridges (Broglio *et al.* 2010). Alternatively, it is possible to calculate the non-linear capacity of bridges on a mechanical basis, although under simplified assumptions. In fact, the energy dissipation capacity of a bridge is concentrated in the piers, if the deck

remains elastic and the bearings do not fail (Fardis 2007). In such conditions, the vulnerability of the bridge can be assessed by studying the piers only, modelled as equivalent SDOF systems, in both the transverse and longitudinal directions. Depending on the direction of the analysis, it is therefore necessary to consider two distinct simplified models characterised by different parameters (Raffaele *et al.* 2014a,b,c), and considering the “effective mass” pertaining to each pier. The shear span of the piers is based on their fixity conditions. Therefore, the Force-Displacement flexural behaviour of a pier is defined by the Moment-Curvature diagram of a critical section, typically located at the base. For a detailed analysis, Moment-Curvature analysis is typically software-based, e.g., KSU\_RC (Esmaeily and Peterman 2007), Cumbia (Montejo and Kowalski 2007), etc. Additional failure mechanisms such as shear, longitudinal bars buckling, lap-slice, second order effects are separately assessed.

However, for regional-scale analyses (Fig. 1) and the derivation of probabilistic fragility curves (Padgett *et al.* 2008, Zelaschi *et al.* 2015, Miano *et al.* 2015), it is useful to have a reliable but rapid solution for the Moment-Curvature diagram related to the RC bridge pier, which is the specific topic of this paper. In particular, a polynomial analytic solution is proposed to retrieve the Moment-Curvature diagram for RC hollow circular sections. This is obtained by means of fitting against hundreds of numerically-based sectional analyses. The result is an accurate, mechanically-based formulation which is rapid and computationally inexpensive at the same time. Alternatively, such a formulation can be used to verify and validate the results of the numerical Moment-Curvature analyses in the context of

\*Corresponding author, Ph.D.

E-mail: [roberto.gentile@poliba.it](mailto:roberto.gentile@poliba.it)

<sup>a</sup>Lecturer

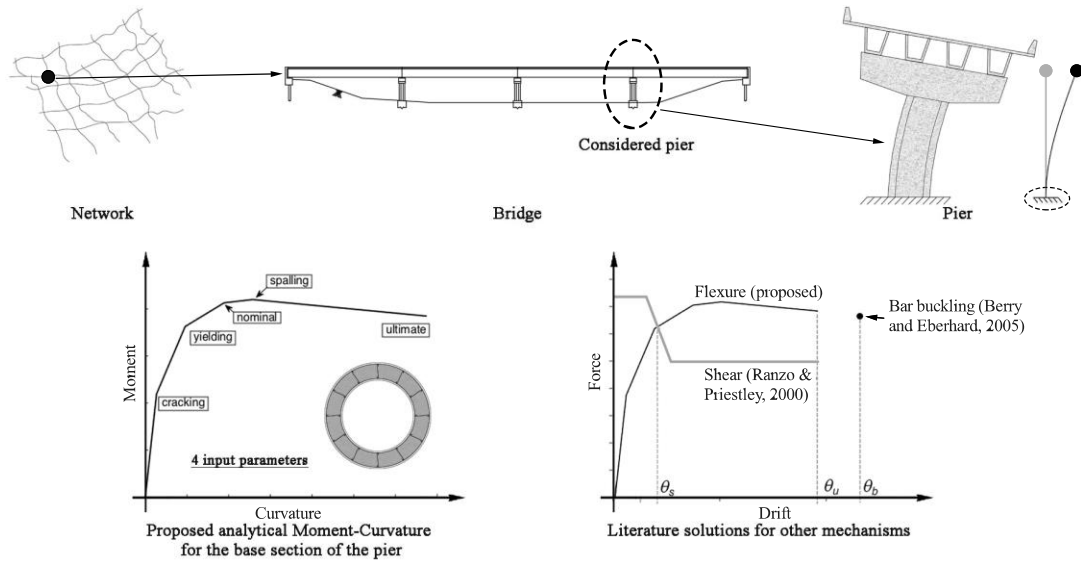


Fig. 1 Adoption of the proposed formulation for the regional scale seismic vulnerability analysis of bridges

detailed analyses on single structures. The assessment is completed by considering the additional mechanisms using analytical literature studies (shear failure, Ranzo and Priestley 2000, longitudinal bars buckling, Berry and Eberhard 2005, lap-splice, Priestley *et al.* 1996, second order effects, Priestley *et al.* 2007).

This simplified solution is deemed to be particularly accurate since it is based on refined stress-strain relationships for concrete and steel. The reliability of the proposed formulation is demonstrated by means of analytical vs numerical scatter plots and by the analysis of a bridge pier case study, comparing the results with refined FEM non-linear analysis.

It is worth mentioning that this work is part of a wider project in which other section shapes have been studied, such as the solid circular shape (Gentile *et al.* 2018), or are currently being studied, such as the rectangular section (Gentile *et al.* 2017).

## 2. Methodology and definition of the simplified formulation

This work is based on the definition of a database that comprises 720 hollow circular RC cross-sections, considering a wide range for the geometrical and mechanical parameters (Section 2.1), particularly appropriate to represent bridge piers cross sections. Four dimensionless parameters are selected, through dimensional analysis, to completely define each case study. A numerically-based Moment-Curvature ( $M-\varphi$ ) analysis is carried out for each entry of the database.

By individuating 6 “characteristic” points (Section 2.2), each numerical ( $M-\varphi$ ) curve is represented by a simplified piecewise linear curve ( $m-\chi$  in dimensionless form), which is deemed to represent the flexural behaviour with sufficient accuracy, if compared to the complete numerical curve. A set of polynomial functions is fitted, by means of a least squares method linear regression, to represent the position

of the characteristic points as a function of the selected dimensionless parameters, whose definition is shown in Eqs. (6)-(9).

### 2.1 Description of the database

Given the number of the involved parameters in the definition of the flexural behaviour of RC hollow circular sections, a number of assumptions is adopted, along with the definition of four dimensionless groups. In general, the involved parameters are: external radius  $R$ , internal radius  $r$ , clear cover  $c$ , axial load  $N$ , concrete unconfined cylindrical compressive strength  $f_c$ , concrete tensile strength  $f_{ct}$ , concrete modulus of elasticity  $E_c$ , yielding strength of longitudinal and transverse reinforcement  $f_{ys}$ ,  $f_{yh}$ , longitudinal and transverse moduli of elasticity of the steel  $E_s$ ,  $E_h$ , respectively, longitudinal reinforcement bars pattern ( $n_l$  and  $d_l$  are the number of bars and their diameter), transverse reinforcement pattern ( $d_h$  and  $s$  are the diameter and the spacing).

For this work, the adopted assumptions are the following:

- concrete tensile strength  $f_t$  (for uniform tensile stress) is assumed to be dependent to the compressive one ( $f_c$ ) according to Eq. (1), provided in the Italian code (NTC 2008). As suggested in the same code, Eq. (2) is adopted to calculate the tensile strength for flexure ( $f_{ct}$ ). Such parameter affects only the first cracking in the Moment-Curvature, therefore this is not likely to limit the scope of the final formulations

$$f_t = 0.3f_c^{2/3} \quad (1)$$

$$f_{ct} = 1.2f_t \quad (2)$$

- according to Eq. (3), the mechanical characteristics of longitudinal and transverse reinforcement steel are the same: yield stress ( $f_{ys}$ ,  $f_{yh}$  respectively) and elastic modulus ( $E_s$ ,  $E_h$  respectively)

$$f_{yh} = f_{ys} \quad \text{and} \quad E_h = E_s \quad (3)$$

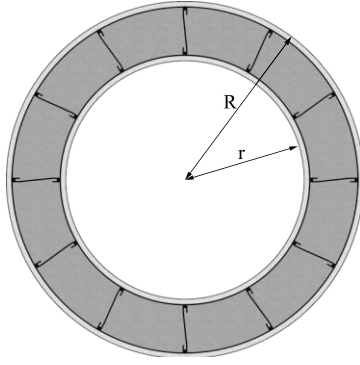


Fig. 2 Cross section and assumed layout of transverse reinforcement

- the longitudinal reinforcement consists of  $n_l/2$  evenly distributed bars of equal diameter ( $d_l$ ) along the internal and external circumferences. The total area of longitudinal steel is defined with Eq. (4)

$$A_s = \frac{n_l(\pi d_l^2)}{4} \quad (4)$$

- the transverse reinforcement pattern, shown in Fig. 2, is composed by two perimetric stirrups and  $n_l/2$  evenly distributed ties. Less-efficient patterns of the stirrups are deemed to be equivalent, in terms of confined concrete performance, to the above-mentioned one with a lower value of the stirrup size  $A_{sp}^{(1)}$ . For this reason, the assumed transverse reinforcement pattern is not deemed to jeopardise the generality of the final polynomial formulations;
- the clear cover,  $c$ , is defined by Eq. (5)

$$c = 0.02R \quad (5)$$

- the diameter is fixed to 1m. This was done considering that the relationship between the curvature at a given limit state and the diameter of the section is linear (e.g., Priestley *et al.* 2007).

Based on dimensional analysis, four dimensionless groups are defined with the remaining parameters, Eqs. (6)-(9): void ratio  $\alpha$ , axial force ratio  $v$ , mechanical ratio of longitudinal reinforcement  $\omega$ , volumetric ratio of transverse reinforcement  $\rho_{sp}$ . Therefore, any hollow circular section in the database can be completely defined with such parameters. Basically, a variation in  $\omega$  can be interpreted as a variation in the longitudinal steel ( $A_s, f_y$ ), the concrete compression strength  $f_c$  or the radii ( $R$  or  $r$ ). Analogously, this applies for the remaining dimensionless groups, also used in similar works (e.g., Perus *et al.* 2006, 2007).

$$\alpha = r/R \quad (6)$$

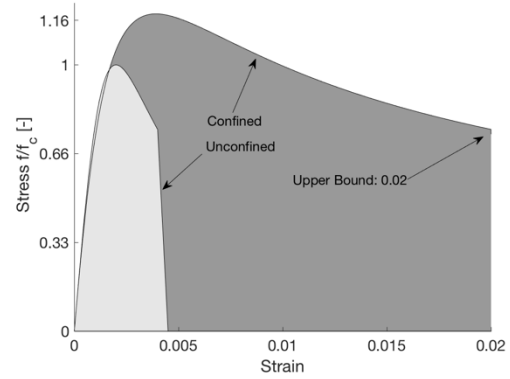
$$v = \frac{N}{\pi(R^2 - r^2)f_c} \quad (7)$$

$$\omega = \frac{A_s f_y}{\pi(R^2 - r^2)f_c} \quad (8)$$

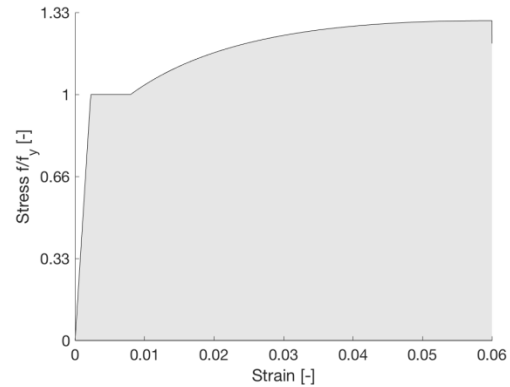
$$\rho_{sp} = \frac{A_{sp}^{(1)}[2\pi(R - c) + 2\pi(r + c) + n_l(R - r - 2c)]}{\pi[(R - c)^2 - (r + c)^2]s} \quad (9)$$

Table 1 Input values for the construction of the database.

Input parameter	Interval		Number of samples
	Min	Max	
$\alpha$	0.6	0.8	3
$v$	0	0.9	10
$\omega$	0.05	0.4	4
$\rho_{sp}$	0	0.04	6



(a) Concrete



(b) Steel

Fig. 4 Assumed stress-strain relationship for the materials

720 numerical analyses are conducted, considering all the possible combinations of the dimensionless parameters shown in Table 1. The range of the input parameters is fine-tuned to include the most probable configurations of RC hollow circular sections typically used in practical applications.

## 2.2 Chosen characteristic points

Six characteristic points are selected for each Moment-Curvature diagram in the database. Those are deemed to be sufficient to represent the flexural behaviour of the cross-section by means of a piecewise linearisation (Fig. 3). Below is given the list of the mechanically-based definition of the characteristic points:

- **Cracking** is the point for which the strain in the furthestmost core concrete fibre is equal to  $\varepsilon_{ct} = f_{ct}/E_c$ ;
- **First Yielding** is related to the tensile yield of the first rebar, or a compressive strain in the furthestmost core concrete fibre equal to  $\varepsilon_c = 0.002$ , whichever occurs first (Priestley *et al.* 2007);

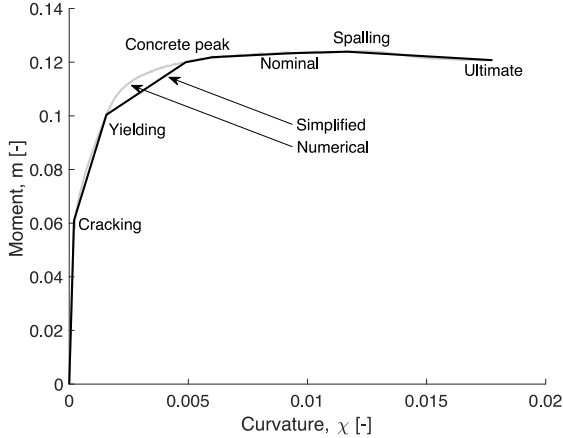


Fig. 3 Definition of the characteristic points

- **Concrete Peak** is associated to the strain corresponding to the peak stress for the furthestmost compressed fibre in the confined core of the section;
- **Nominal**. This corresponds to a compressive strain equal to  $\varepsilon_c = 0.004$  in the furthestmost core concrete compression fibre or equal to  $\varepsilon_s = 0.015$  in the furthestmost tension rebar, whichever occurs first (Priestley *et al.* 2007);
- **Spalling** is the point on the ( $M$ - $\chi$ ) diagram for which the strain of the unconfined concrete in the cover it's equal to its ultimate strain (0.0045). Typically, this is associated to a degrading branch in the ( $M$ - $\chi$ ) diagram;
- The **Ultimate** point corresponds to the ultimate compressive strain for confined concrete (according to Mander *et al.* 1988) or the ultimate tensile strain for steel (assumed to be 0.06, according to NZSEE 2017).

## 2.2 Assumptions for the numerical analyses

A *Moment-Curvature* analysis is conducted for each entry of the database, considering all the combinations of the selected input parameters ( $3 \times 10 \times 4 \times 6 = 720$  combinations). The software KSU-RC (Esmaily and Peterman 2007) is adopted for the Moment-Curvature analyses, which is based on a fibre discretisation of the cross-section.

Concrete is modelled according to (Mander *et al.* 1988), considering both the confined and unconfined behaviour (Fig. 4(a)). It is worth mentioning that the confined concrete ultimate strain is calculated according to Mander *et al.* 1988, adopting 0.02 as an upper bound value.

The behaviour of steel (Fig. 4(b)) is modelled according to Esmaily and Peterman, 2007. The curve is linear up to yielding, with a plateau up to 10 times the yielding strain (Sadowski *et al.* 2017) and followed by a parabolic shape up to the ultimate strain, which corresponds to the peak and is equal to 0.06 to implicitly consider low cycle fatigue failure (NZSEE 2017). The peak stress is assumed to be 1.3 times the yield stress. These parameters are tuned to represent a commercial steel with a nominal yield stress ranging between 400 and 500 MPa, e.g., the Italian B450C (NTC 2008) or the New Zealand grade 500 (NZSEE 2017). It is worth mentioning that the adopted stress-strain

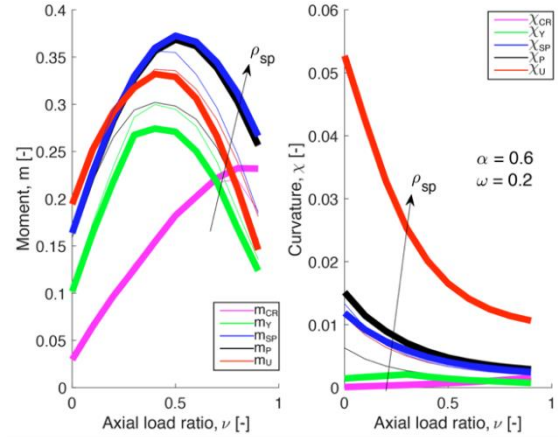


Fig. 5 Trends for the ultimate moment and curvature: section void ratio  $\alpha=0.6$ , longitudinal reinforcement ratio  $\omega=0.2$

relationship is in close agreement with the widely utilised curve proposed in King *et al.* (1986), as shown in Gentile *et al.* (2018).

## 3. Analysis of the trends and accuracy of the polynomials

### 3.1 Post processing and curve fitting

Each Moment-Curvature diagram in the database is firstly expressed in dimensionless form according to Eqs. (10) and (11). Therefore, a purpose-specific Matlab routine is used to “extract” the characteristic points, both in terms of moment and curvature. Fig. 5 shows, as an example, the trend of the characteristic moments and curvatures as a function of the dimensionless axial force,  $\nu$ , a fixed value of both the void ratio ( $\alpha$ ) and the longitudinal reinforcement ( $\omega$ ) and the minimum and maximum value of the transverse reinforcement ( $\rho_{sp}$ ) ratios (represented by the thickness of the line). Appendix A shows the synthetic plots considering the entire database. In such plots (Fig. 9 and Fig. 10), void ratio ( $\alpha$ ) and the mechanical ratio of the longitudinal reinforcement ( $\omega$ ) is fixed, each characteristic point has a different line colour (e.g., green is for yielding), and the line width increases with the increase of the volumetric ratio of transverse reinforcement (the dashed line is for unconfined).

$$m = \frac{M}{\pi(1 - \alpha^2)R^3 f_c} \quad (10)$$

$$\chi = \phi R \quad (11)$$

A set of polynomial functions is fitted using a least square method linear regression, using the extracted characteristic moments and curvatures in the database. The input variables for these polynomials are the four dimensionless input parameters defined in Section 2.1. This process led to 14 polynomials, in the form of Eq. (12) and (13), which allow to analytically construct the Moment-Curvature diagram of hollow circular sections characterised by mechanical and geometrical parameters within the scope

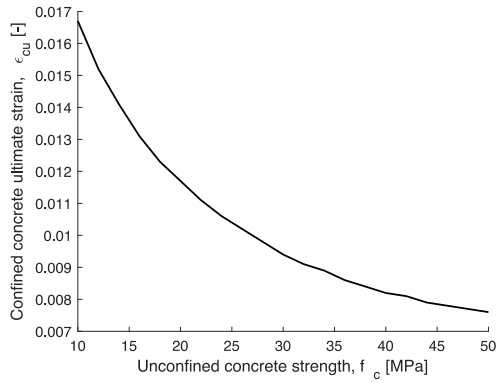


Fig. 3 Relationship between unconfined concrete strength and confined concrete ultimate strain for a given value of the transverse reinforcement ratio ( $\rho_{sp}=0.01$ )

of this database.

The study of the main trends (Fig. 9-Fig. 10) allowed to select the degree of the polynomials with respect to the four selected input parameters. The *adjusted* -  $R^2$  value is greater than 95% for all the polynomials. Although this is not a statistical analysis, the terms with a *p* - value smaller than 5% are eliminated.

$$\begin{aligned}
 m_{char} = & a_0 + a_1\alpha + a_2v + a_3\omega + a_4\rho_{sp} + a_5\alpha^2 \\
 & + a_6v^2 + a_7\omega v + a_8\omega^2 + a_9v\rho_{sp} + \\
 & a_{10}\omega\rho_{sp} + a_{11}\alpha v + a_{12}\alpha\omega + a_{13}\alpha\rho_{sp} + a_{14}\alpha^2v \\
 & + a_{15}\alpha v^2 + a_{16}\alpha\omega^2 + a_{17}\alpha^2\omega + a_{18}\alpha\rho_{sp}^2 \quad (12) \\
 & + a_{19}\alpha v\omega + a_{20}\alpha\omega\rho + a_{21}\alpha v\rho_{sp} + a_{22}v^3 + a_{23}v^2\omega \\
 & + a_{24}v\omega^2 + a_{25}v\rho_{sp}^2 + a_{26}v^2\rho_{sp} + a_{27}v\omega\rho_{sp} \\
 & + a_{28}\omega\rho_{sp}^2 + a_{29}\omega^2\rho_{sp} + a_{30}\rho_{sp}^2
 \end{aligned}$$

$$\begin{aligned}
 \chi_{char} = & a_0 + a_1\alpha + a_2v + a_3\omega + a_4\rho_{sp} + a_5\alpha^2 \\
 & + a_6v^2 + a_7\omega v + a_8\omega^2 + a_9v\rho_{sp} \\
 & + a_{10}\omega\rho_{sp} + a_{11}\alpha v + a_{12}\alpha\omega + a_{13}\alpha\rho_{sp} \quad (13) \\
 & + a_{14}\alpha^2v + a_{15}\alpha v^2 + a_{16}\alpha^2\omega + a_{17}\alpha v\omega \\
 & + a_{18}\alpha v\rho_{sp} + a_{19}v^3 + a_{20}v^3\rho_{sp} + a_{21}v^2\omega + a_{22}v\omega^2 \\
 & + a_{23}v^2\rho_{sp} + a_{24}v\omega\rho_{sp} + a_{25}\omega^2\rho_{sp} + a_{26}\rho_{sp}^2
 \end{aligned}$$

### 3.2 Ultimate curvature correction factor

A constant value equal to  $f_c = 31.83$  MPa is considered in the database. Therefore, an additional process is adopted to consider the variability of the ultimate curvature with respect to this parameter. Confined concrete ultimate strain depends on the unconfined concrete compressive strength, according to Mander *et al.* (1986). Given the ratio of transverse reinforcement, the relationship between confined concrete ultimate strain and unconfined concrete compressive strength is parabolic and it is shown in Fig. 6. A similar pattern is to be expected for the ultimate curvature, that directly depends on the ultimate strain.

This effect is taken into account with a correction factor for the ultimate curvature, calibrated through a sensitivity analysis with respect to  $f_c$ . A smaller database of RC sections is defined in which the parameters  $\alpha$ ,  $v$ ,  $\omega$  and  $\rho_{sp}$  are constant while  $f_c$  is variable. The dimensionless ultimate dimensionless curvature  $\chi_u(f_c)$  is calculated for

each of them by means of a numerical Moment-Curvature analysis and the post processing. On the other hand, the calibrated polynomial for the ultimate curvature, Eq. (13), is used to predict the same value, named  $\chi_u(31.83)$ . The ‘‘Correction Factor (CF)’’, Eq. (14), is therefore fitted against the ratios of the above-mentioned parameters. This is used to include the variability of the ultimate curvature with the concrete strength, according to Eq. (15), by multiplying the value predicted with the ultimate curvature polynomial (depending on  $\alpha$ ,  $v$ ,  $\omega$ ,  $\rho_{sp}$ ) to the correction factor (which depends on  $f_c$ ).

$$CF = \frac{\chi_u(f_c)}{\chi_u(31.83)} = 0.000276f_c^2 - 0.032f_c + 1.7453 \quad (14)$$

$$\chi_u(f_c) = CF\chi_u(31.83) \quad (15)$$

### 3.3 Reliability of the polynomials

A specific procedure is adopted to validate the proposed simplified polynomials for the construction of ( $M - \varphi$ ) diagrams. A set of 14 RC hollow circular sections (‘‘test cases’’), not included in the original database, is defined considering configurations appropriate for RC bridge piers. According to the same procedure used for the database, the test cases are analysed to obtain the characteristic moments and curvatures. The geometrical and mechanical characteristics of the test dataset is shown in Table 6, in Appendix A. The same parameters are predicted using the proposed polynomial solution, also considering the ultimate curvature correction factor.

For each test case, the error for the 14 polynomials is calculated with Eq. (16) and a global error ( $ERR_{glob}$ ) is calculated using Eq. (17). The results (Table 2) show that the error is smaller than 11% except for the ultimate curvature for which it is equal to 16.8%. Finally, the general trends for the polynomials are shown in the analytical (predicted) vs numerical (‘‘measured’’) plots in Fig. 7, considering both the original database and the test series. This demonstrates the accuracy of the proposed model, considering the relatively low registered scatter regardless of the considered characteristic polynomial.

$$Err = 100 \left| \frac{analytical - numerical}{numerical} \right| \quad (16)$$

$$Err_{glob} = \frac{\sum_{i=1}^{14} Err_i}{14} \quad (17)$$

## 4. Application to a case study bridge pier

A numerical validation of the proposed polynomial formulation is presented herein. An RC bridge pier case

Table 2 Percentage global error for the test dataset

	$\chi_{CR}$	$\chi_{Yc}$	$\chi_Y$	$\chi_P$	$\chi_N$	$\chi_{SP}$	$\chi_U$	$m_{CR}$	$m_{Yc}$	$m_Y$	$m_P$	$m_N$	$m_{SP}$	$m_U$
$ERR_{glob}$	2.3	10.9	6.2	1.2	8.8	6.3	16.8	1.5	2.1	3.6	3.2	3.0	2.6	7.3

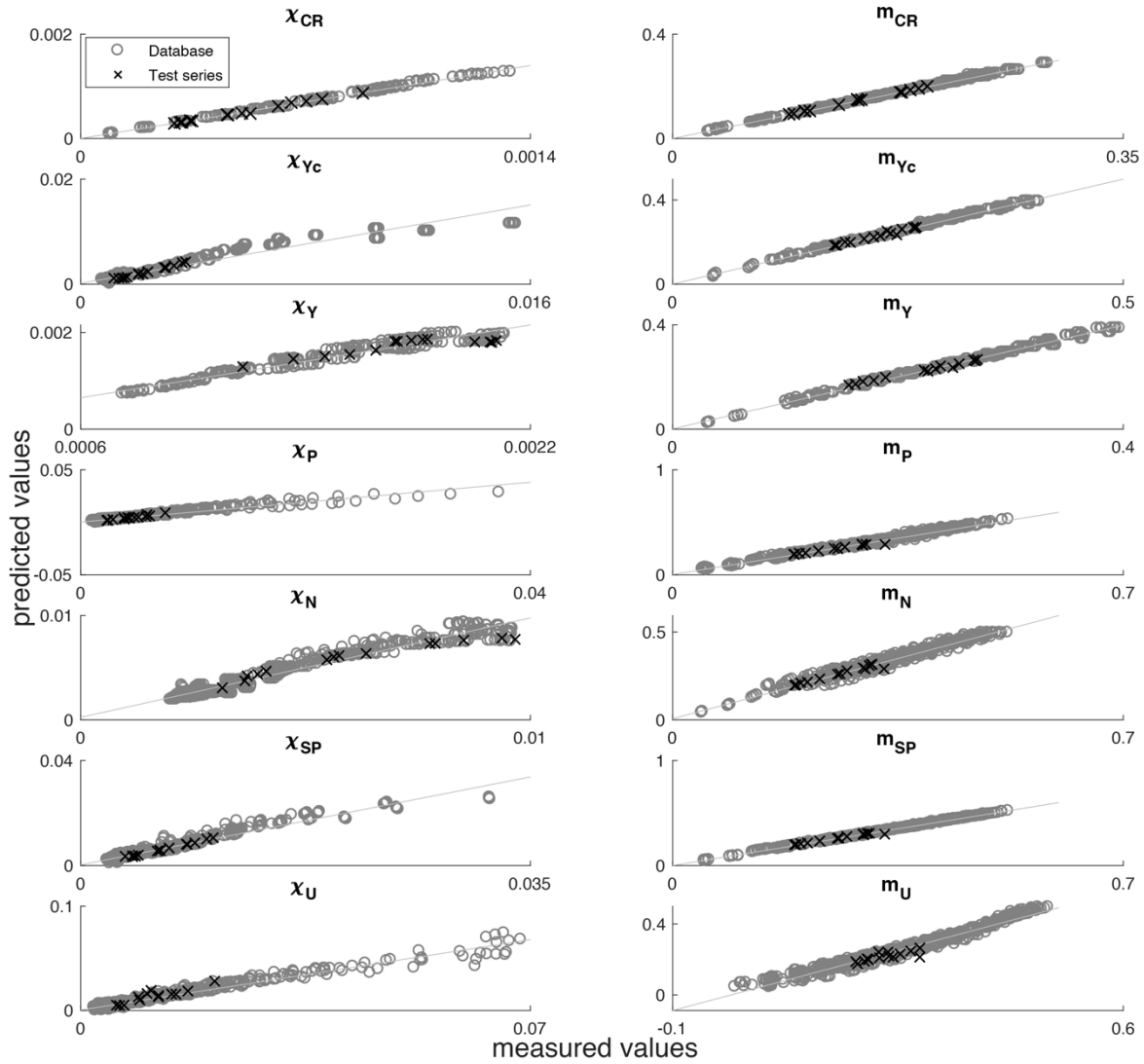


Fig. 7 Predicted vs “measured” (numerical) plots for the characteristic polynomials

Table 3 Geometrical and mechanical characteristics of the case study

$L$	$R$	$r$	$c$	$n_l$	$d_l$	$d_h$	$s$	$f_c$	$f_{ys}$	$N$	$\alpha$	$\nu$	$\omega$	$\rho_{sp}$
[m]	[m]	[m]	[m]	[-]	[mm]	[-]	[mm]	[MPa]	[MPa]	[MN]	[-]	[-]	[-]	[-]
8	2.2	1.6	0.05	40	20	12	100	20	430	10	0.727	0.279	0.151	0.006

study with hollow circular cross-section is analysed. The geometrical and mechanical parameters belonging to the piers are listed in Table 3. It should be recognised that the length and the axial load on the simplified SDOF representing the pier depend, in general, on the fixity conditions of the bridge and the “effective mass” pertaining to the pier itself.

The proposed polynomials, Eqs. (12) and (13), are used to predict the flexural behaviour of the base section of the pier. Eqs. (10) and (11) are used to transform the result in dimensional form. This is shown in Fig. 8(a), where the curve is compared to the numerical solution obtained with SAP2000 v18 section designer (Computers and Structures 2016). A particularly good match is shown, with a slight underestimation of the ultimate moment and curvature (3.9% and 6.0%, respectively).

The Force-Displacement ( $F - \delta$ ) curve (Fig. 8(b)) is calculated according to Eqs. (18) and (19), in which  $\varphi$  is the curvature,  $\varphi_Y$  is the yield curvature,  $M$  is the moment,  $L$  is the length of the pier and  $L_p$  ( $= 0.67$  m) is the plastic hinge length, calculated according to Priestley and Park, (1987). On the other hand, the pier is modelled using 8 “beam” elements in the FEM software SAP2000 v18. 600 fibres are used to discretise the cross-section using the “Fiber P M2 M3 hinge” property in the software. The constitutive relationships shown in Fig. 4 are used for the materials. A displacement-control Pushover analysis is conducted applying a horizontal force at the top of the pier.

The numerically-based flexural capacity curve is compared to the analytical one (Fig. 8(b)) showing that the two approaches are matching. A 1.6% and 6.1% overestimation is respectively registered for the force and

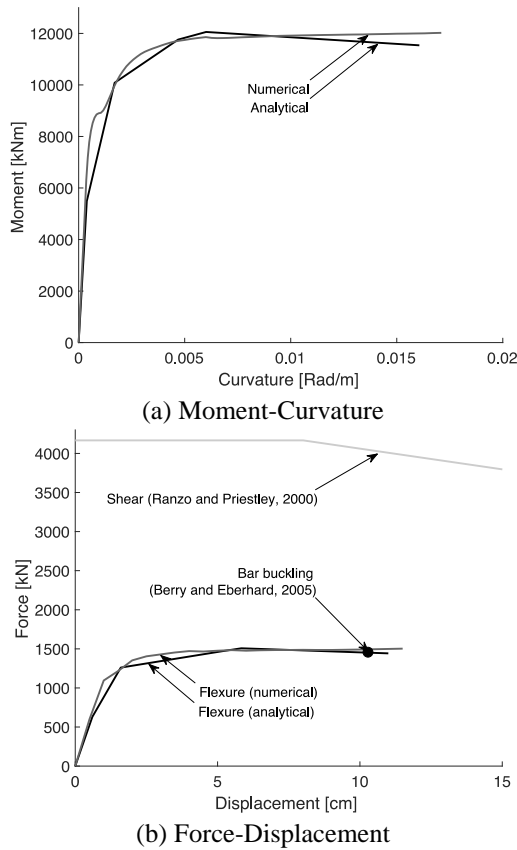


Fig. 8 Practical application: comparison between analytical and numerical solutions

the displacement at the peak, while for the ultimate force and displacement, a 4.0% and 4.3% underestimation is respectively measured.

Fig. 8(b) shows the shear degradation curve calculated according to Ranzo and Priestley (2000) and the bar buckling displacement, calculated according to Berry and Eberhard (2005). The predicted failure mode for the pier is bar buckling, since the shear degradation curve is not intersecting the flexural one, and the bar buckling displacement is smaller than the ultimate flexural one.

$$\delta = \begin{cases} \frac{\varphi L^2}{3} & \text{if } \varphi \leq \varphi_Y \\ \frac{\varphi_Y L^2}{3} + (\varphi - \varphi_Y)L_p(L - 0.5L_p) & \text{if } \varphi > \varphi_Y \end{cases} \quad (18)$$

$$F = \frac{M}{L} \quad (19)$$

## 5. Conclusions

In this paper, a polynomial solution for the characterisation of the flexural behaviour of RC hollow circular cross-sections is proposed, with particular reference to bridge piers. The *Moment-Curvature* diagram is calculated by defining the position of six characteristic points, related to mechanically-based performance points (e.g., cover spalling). Calibrated polynomials allow to

accomplish this goal. Those are dependent on four parameters: section void ratio, dimensionless axial force, mechanical ratio of longitudinal reinforcement, volumetric ratio of transverse reinforcement. The polynomial functions are fitted against a database of 720 fibre-based numerical *Moment-Curvature* diagrams which considers wide ranges for the defining parameters. An RC bridge pier case study is assessed using the proposed formulation and the results are compared to a refined non-linear FEM model showing good match.

The scope of the proposed polynomial formulation is the regional scale seismic assessment of multi-span bridges with RC hollow circular piers, based on a mechanical approach, instead of the commonly-used empirical methods based on calibrated indices. While allowing accuracy, this simple method allows to considerably reduce the computational effort for large number of analyses, since it's implementable in computer-based electronic spreadsheets. This work is part of a wider project, which considers solid circular sections and aims to study other significant section shapes in the future.

## Acknowledgments

The research described in this paper was partially supported by the Project ReLUIS-DPC 2014-2018, "Linea C.A."-R.U. Politecnico di Bari (G. Uva) and the FRA 2016 project (Politecnico di Bari, D. Raffaele).

## References

- Berry, M.P. and Eberhard, M.O. (2005), "Practical performance model for bar buckling", *J. Struct. Eng.*, **131**(7), 1060-1070.
- Broglio, S., Crowley, H. and Pinho, R. (2010), "Simplified capacity curves for RC bridges", *Proceedings of 14<sup>th</sup> European Conference on Earthquake Engineering*, Ohrid, Republic of Macedonia.
- Computer and Structures (2016), SAP2000 v18, Structural Analysis Program, Manual, Berkeley, California, USA
- Esmaili, A. and Peterman, R.J. (2007), "Performance analysis tool for reinforced concrete members", *Comput. Concrete*, **4**(5), 331-346.
- Fardis, M.N. (2007), "Risk mitigation for earthquakes and landslides. Guidelines for displacement-based design of buildings and bridges", Report No. 5/2007, IUSS Press, Pavia, Italy.
- Gentile, R., Porco, F., Raffaele, D. and Uva, G. (2018), "Simplified Moment-Curvature relationships in analytical form for circular RC sections", *Bull. NZ Soc. Earthq. Eng.*, **51**(3).
- Gentile, R., Raffaele, D. and Uva, G. (2017), "Simplified polynomial formulation for the calculation of the Moment-Curvature diagram of RC rectangular sections", *Proceedings of the XVII Italian Conference On Seismic Engineering*, Pistoia, Italy, September.
- King, D.J., Priestley, M.J.N. and Park, R., (1986), "Computer programs for concrete column design", Research Report 86/12, Department of Civil Engineering, University of Canterbury, Christchurch, New Zealand.
- Kircher, C.A., Whitman, R.V. and Holmes, W.T. (2006), "HAZUS Earthquake Loss Estimation Methods", *Nat. Hazard Rev.*, **7**, 45-59.
- Mander, J.B., Priestley, M.J.N. and Park, R. (1988), "Theoretical

- stress strain model for confined concrete”, *J. Struct. Eng.*, **114**(8), 1804-1826.
- Miano, A., Fatemeh, J., De Risi, R., Prota, A. and Manfredi, G. (2015), “A case-study on scenario-based probabilistic seismic loss assessment for a portfolio of bridges”, *Proceedings of the 12th International Conference on Applications of Statistics and Probability in Civil Engineering, ICASP12*, Vancouver, Canada.
- Montejo, L.A. and Kowalsky, M.J. (2007), “Set of codes for the analysis of reinforced concrete members”, Technical Report No. IS-07-01, North Carolina State University, USA.
- NTC (2008), Ministero delle Infrastrutture e dei Trasporti “DM 14 gennaio 2008 in materia di “norme tecniche per le costruzioni”, Gazzetta ufficiale n.29 del 4 febbraio 2008, Supplemento ordinario n.30”, Istituto Poligrafico e Zecca dello stato.
- NZSEE/MBIE (2017), “The seismic assessment of existing buildings technical guidelines for engineering assessments”, Final draft 1, July, New Zealand.
- Padgett, J.E., Nielson, B.G. and Desroches, R. (2008), “Selection of optimal intensity measures in probabilistic seismic demand models of highway bridge portfolios”, *Earthq. Eng. Struct. Dyn.*, **37**, 711-725.
- Palermo, A., Liu, R., Rais, A., McHaffie, B., Andisheh, K., Pampanin, S., Gentile, R., Nuzzo, I., Graniero, M., Loporcaro, G., McGann, C. and Wotherspoon, L. (2017), “Performance of road bridges during the 14<sup>th</sup> November 2016 Kaikoura earthquake”, *Bull. NZ Soc. Earthq. Eng.*, **50**(2), 253-270.
- Peruš, I. and Fajfar, P. (2007), “Prediction of the force-drift envelope for RC columns in flexure by the CAE method”, *Earthq. Eng. Struct. Dyn.*, **36**(15), 2345-2363.
- Peruš, I., Poljanšek, K. and Fajfar, P. (2006), “Flexural deformation capacity of rectangular RC columns determined by the CAE method”, *Earthq. Eng. Struct. Dyn.*, **35**(12), 1453-1470.
- Pinho, R., Monteiro, R., Casarotti, C. and Delgado, R. (2009), “Assessment of continuous span bridges through nonlinear static procedures”, *Earthq. Spectra*, **25**(1), 143-159.
- Priestley, M.J.N. and Park, R. (1987), “Strength and ductility of concrete bridge columns under seismic loading”, *ACI Struct. J.*, **84**(1), 61-76.
- Priestley, M.J.N., Calvi, G.M. and Kowalsky, M.J. (2007), *Displacement based Seismic Design of Structures*, IUSS Press, Pavia, Italy.
- Priestley, M.J.N., Seible, F. and Calvi, G. (1996), *Seismic Design and Retrofit of Bridges*, John Wiley and Sons, New York, USA.
- Raffaele, D., Porco, F., Fiore, A. and Uva, G. (2014a), “Simplified vulnerability assessment of reinforced concrete circular piers in multi-span simply supported bridges”, *Struct. Infrastr. Eng.*, **10**(8), 950-962.
- Raffaele, D., Porco, F., Uva, G. and Fiore, A. (2014b), “Simplified assessment of seismic retrofitting interventions on RC circular piers in multi-span simply supported bridges”, *Proceedings of the 7th International Conference on Bridge Maintenance, Safety and Management*, Shanghai, China.
- Raffaele, D., Uva, G., Porco, F. and Fiore, A. (2014c), “About of seismic capacity of bridge piers: A simplified approach”, *Proceedings of the 7th International Conference on Bridge Maintenance, Safety and Management*, Shanghai, China.
- Ranzo, G. and Priestley, M.J.N. (2000), “Seismic performance of large RC circular hollow columns”, *Proceedings of the 12<sup>th</sup> World Conference on Earthquake Engineering*, Auckland, New Zealand, February.
- Sadowski, A.J., Rotter, J.M., Stafford, P.J., Reinke, T. and Ummenhofer, T. (2017), “On the gradient of the yield plateau in structural carbon steels”, *J. Constr. Steel Res.*, **130**, 120-130.
- Zelaschi, C., Monteiro, R. and Pinho, R. (2015), “Improved fragility functions for RC bridge populations”, *Proceedings of the 5th ECCOMAS Thematic Conference on Computational Methods in Structural Dynamics and Earthquake Engineering*, Crete Island, Greece, May.

AT



Table 6 Geometric and mechanical characteristics for the test dataset

$D$ [m]	$r$ [m]	$c$ [m]	$n_l$ [-]	$d_l$ [mm]	$d_h$ [mm]	$s$ [mm]	$f_c$ [MPa]	$f_{ys}$ [MPa]	$N$ [MN]	$\alpha$ [-]	$\nu$ [-]	$\omega$ [-]	$\rho_{sp}$ [-]
1.35	0.85	0.06	30	26	10	100	45	370	20	0.630	0.129	0.038	0.008
1.30	0.80	0.06	40	24	8	60	24	350	21	0.615	0.265	0.080	0.009
1.45	0.97	0.05	42	28	10	50	30	380	32	0.669	0.292	0.090	0.017
1.23	0.75	0.05	44	22	12	80	28	400	25	0.612	0.310	0.081	0.018
1.40	0.90	0.04	36	24	16	120	25	450	55	0.643	0.609	0.081	0.016
1.50	1.00	0.04	38	26	10	90	39	500	25	0.667	0.163	0.066	0.008
1.60	1.10	0.04	46	30	14	70	32	480	21	0.688	0.159	0.115	0.022
1.75	1.25	0.04	40	32	12	50	29	360	45	0.714	0.329	0.085	0.020
1.90	1.40	0.07	46	26	8	60	26	390	63	0.737	0.471	0.071	0.008
2.00	1.50	0.07	44	24	10	65	32	450	31	0.750	0.176	0.051	0.012
1.80	1.40	0.04	36	30	12	75	31	490	53	0.778	0.425	0.100	0.015
1.55	0.95	0.05	50	22	10	80	40	380	60	0.613	0.318	0.038	0.010
1.85	1.35	0.06	46	30	14	60	25	450	75	0.730	0.597	0.116	0.025
2.05	1.55	0.04	42	26	12	80	28	420	64	0.756	0.408	0.059	0.012

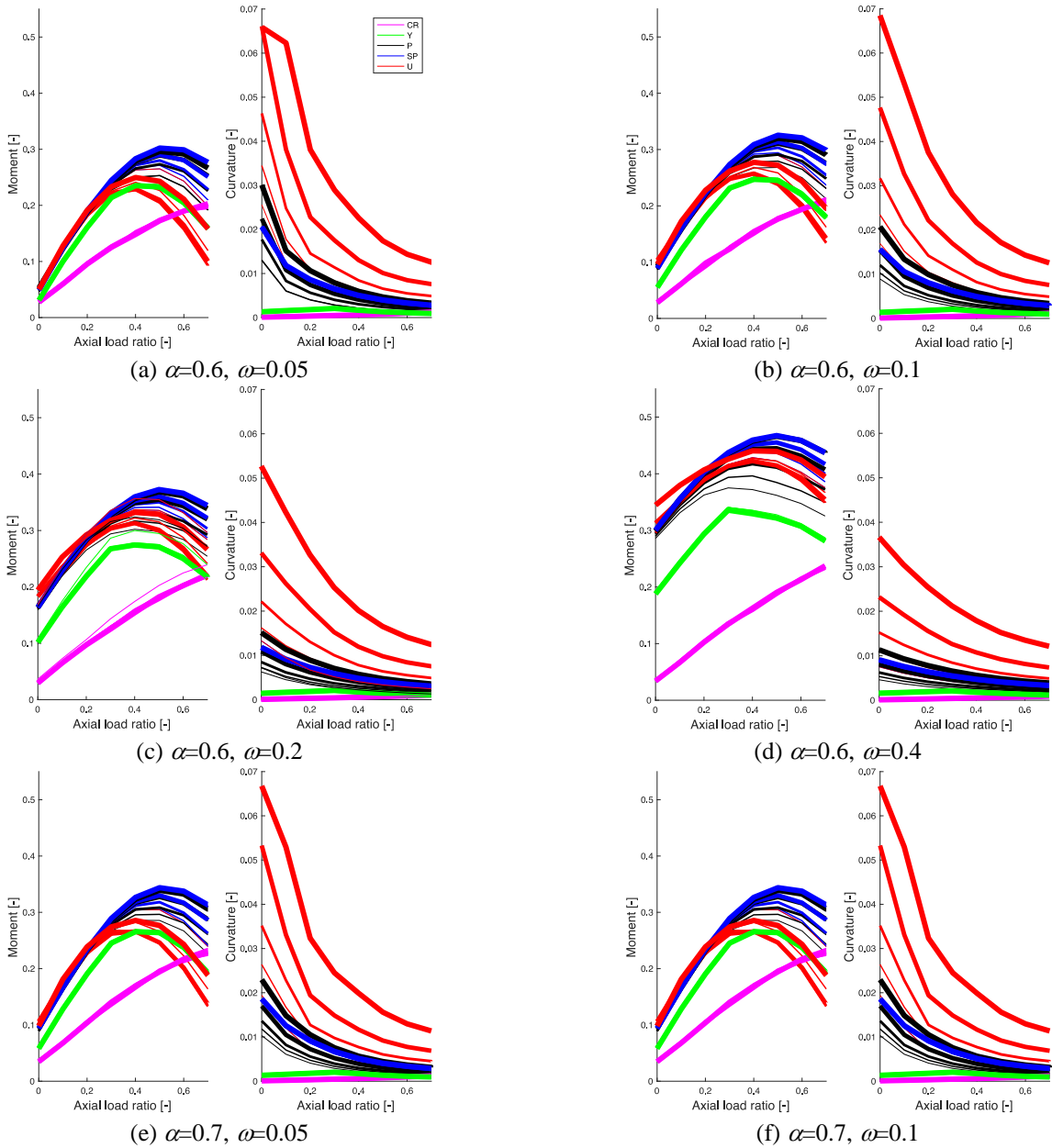


Fig. 9 Main trends for the characteristic moments and curvatures

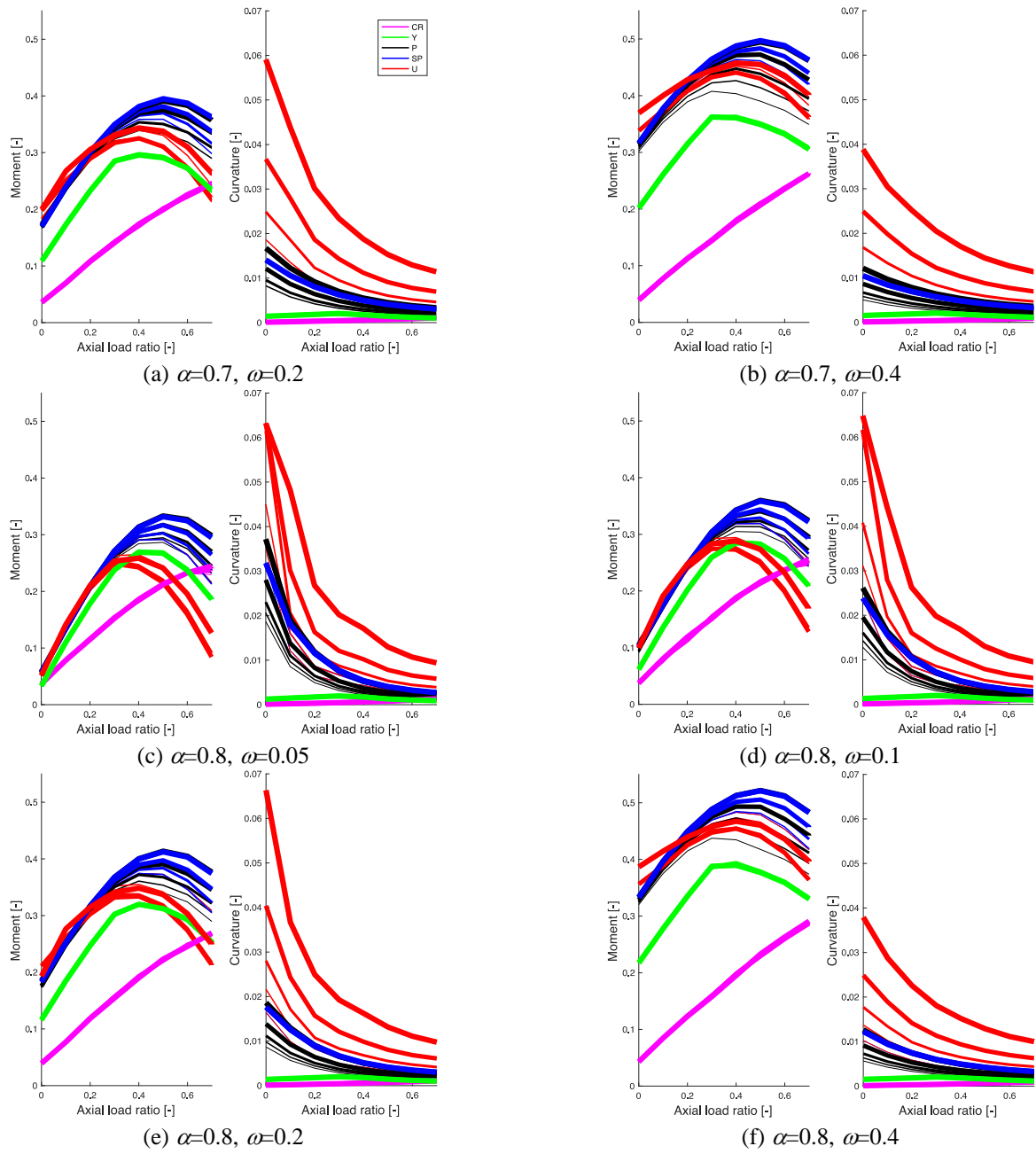


Fig. 10 Main trends for the characteristic moments and curvatures